Journal of Pharmaceutical and Medical Research
Print ISSN: 2663-1954
Online ISSN: 2663-1962
DOI: https://doi.org/10.61784/jpmr3106

HEAT-MASS COUPLED SIMULATION OF CYLINDRICAL HERBAL MEDICINE IN HOT-AIR PREHEATING STAGE

YinKai Guo
School of Mathematics and Physics, North China Electric Power University, Beijing 102206, China.

Abstract: Aiming at the preheating-balance phase in hot-air drying of cylindrical Chinese herbal medicines, a one-dimensional axisymmetric heat-mass coupled diffusion model is established based on mass conservation and energy conservation to reveal the spatio-temporal evolution of internal temperature and moisture concentration fields. Normalized coordinate transformation is adopted for the cylindrical radial computational domain, and the fully-implicit finite volume method combined with the Thomas algorithm is applied to discretize and solve governing equations. Linear interpolation preprocessing is performed on raw time-series environmental data of the drying chamber to eliminate non-physical oscillations caused by step-shaped boundaries. Numerical results show that the temperature field responds rapidly in the preheating stage. At 1800 s, the central temperature reaches 33.5742 °C and the surface temperature reaches 36.7841 °C, and the internal-external temperature difference decreases obviously. Moisture migration is only confined to the surface layer within 0.5 cm, while internal moisture content basically remains at the initial value. Comparisons with analytical series solutions of cylindrical unsteady heat conduction as well as grid-independence and time-step convergence tests are carried out. The maximum absolute temperature error is only 1.20×10^{-3} °C, which verifies the reliability of the proposed model and numerical scheme. This model provides theoretical support for parameter selection of preheating processes for Chinese herbal medicine drying.
Keywords: Chinese herbal medicine drying; Heat-mass coupling; One-dimensional axisymmetry; Finite volume method; Preheating stage

1 INTRODUCTION

Hot-air drying is a widely-adopted processing technology for Chinese herbal medicines, and the preheating-balance phase largely determines subsequent drying performance and final product quality [1-3]. During preheating, complex coupled heat-mass transfer takes place inside cylindrical herbal materials, forming non-uniform spatial distribution of temperature and moisture. Improper preheating parameters may trigger surface hardening, internal stress and uneven dehydration, which impair medicinal value and storage stability [4-5]. Even minor deviation in preheating temperature can further shift the timing of internal moisture migration and change the whole drying schedule. Physical experiments for process optimization consume substantial manpower and material resources, and destructive sampling is usually required to obtain internal field data. Establishing reliable numerical models to reveal transient field evolution has become an effective auxiliary means for drying-process design [6-7].

Extensive research has focused on drying-kinetic simulation of porous biological materials [8-10]. Most existing studies concentrate on the full drying cycle or late-stage falling-rate dehydration, while less attention is paid to independent modelling of the short preheating-balance stage. Many numerical works directly adopt step-form boundary conditions from original environmental monitoring data, which easily produces non-physical oscillation near material surfaces. Moreover, analytical solutions are only valid under constant-property and ideal boundary assumptions, and cannot handle time-varying actual hot-air conditions. Most existing simulation frameworks tend to couple variable-property parameters from the very beginning and bring extra computational overhead for short-term preheating calculation. Few publications combine normalized coordinate transformation with fully-implicit finite-volume discretization to accurately capture fast-response temperature fields and slow-evolving moisture fields in the preheating phase.

Targeting the above research gaps, this paper constructs a one-dimensional axisymmetric heat-mass coupled diffusion model for cylindrical Chinese herbal medicines under constant thermophysical properties. Linear-interpolation preprocessing is implemented for time-series environmental data to eliminate step-induced numerical oscillation. The fully-implicit finite-volume method together with the Thomas algorithm is applied to solve transient temperature and moisture fields. Grid-independence tests, time-step convergence verification and comparison with analytical series solutions are conducted to validate numerical accuracy. This work provides quantitative transient-field references and simulation frameworks for parameter optimization of the preheating stage in herbal-medicine hot-air drying.

2 METHODOLOGY

2.1 Detailed Analysis

This problem is a mechanism analysis forward problem under constant thermophysical properties and fixed geometry. It aims to solve the spatio-temporal evolution of internal temperature and dry-basis moisture content fields inside herbal

© By the Author(s) 2026, under the CC BY-NC-ND license (http://creativecommons.org/licenses/by-nc-nd/4.0).

materials with known time-series temperature and humidity data of the drying chamber and constant property parameters. A one-dimensional axisymmetric heat-mass coupled diffusion equation is adopted and solved by the finite volume method with fully implicit time integration.

First, numerical cleaning and linear interpolation resampling are performed on the temperature and humidity time series to obtain continuous environmental conditions consistent with the output grid. Then, heat conduction and water diffusion equations in cylindrical coordinates are established based on energy conservation and mass conservation, together with central symmetry conditions, surface convective boundary conditions and initial conditions. A normalized radial coordinate is introduced to rewrite the governing equations into conservation form. The finite volume method is used for integration over radial control volumes to derive semi-discrete equations. The backward Euler scheme is applied for temporal discretization, transforming the equations into a tridiagonal system of linear equations. Finally, a band matrix solver is used for time marching. The solutions at control volume centers are interpolated onto the grid specified by the problem to output results.

2.2 Model Preparation

2.2.1 Data preprocessing

The drying chamber temperature and water concentration provided are sampled at equal intervals of 60 s, with a total of 241 observation points covering a time range of 0 ~ 14400 s. The formal numerical solution adopts a time step of 0.25 s, and results are output at a resolution of 1 s and 0.1 cm as required. If the original sequence is assigned in a stepwise manner, boundary conditions remain constant within each sampling interval, causing artificial jumps in surface flux and introducing non-physical oscillations in the early evolution of both fields. Therefore, numerical cleaning and consistency verification are carried out first: convert the three columns of time, temperature and water concentration into numerical values, remove empty values, sort in ascending time order and eliminate duplicate records, verifying that the time axis is strictly monotonic. Linear interpolation resampling is then performed. Let the original sampling time be t_i and the corresponding observation value be y_i (where y denotes temperature or water concentration). The interpolation result at any time $t \in [t_i, t_{i+1}]$ is:

$$y(t) = \frac{t_{i+1}-t}{t_{i+1}-t_i} y_i + \frac{t-t_i}{t_{i+1}-t_i} y_{i+1}, \quad t_i \le t \le t_{i+1} \tag{1}$$

where y_i represents the drying chamber temperature or water concentration at the i-th sampling moment. On this basis, a unified environmental condition function is constructed and saved as a preprocessed data file on a 60 s grid.

2.2.2 Algorithm selection

After the environmental boundary conditions are continuous, a numerical solution scheme is selected for the governing equations. Five candidate methods, including analytical solution, explicit finite difference method, explicit finite volume method, fully implicit finite volume method and finite element method, are compared from three dimensions: nonlinear adaptability, stability and computational efficiency, as shown in Table 1.

Table 1 Comparison of Solution Algorithms

Algorithm	Nonlinear adaptability	Stability	Computational efficiency
Analytical series solution	Poor	Good	Good
Explicit finite difference	Medium	Poor	Medium
Explicit finite volume	Medium	Medium	Medium
Fully implicit finite volume	Good	Good	Good
Finite element method	Good	Good	Poor

As shown in Table 1, analytical series solutions are only applicable under constant thermophysical properties and constant boundary conditions, and cannot handle nonlinear diffusion coefficients varying with moisture content. Explicit schemes are limited by stability conditions $\Delta t \le \Delta r^2/(2\alpha)$, requiring extremely small time steps for long-time marching. Although the finite element method is versatile, the geometry and boundary conditions in this problem are simple, so its implementation complexity is disproportionate to the benefit. Therefore, the fully implicit finite volume method is selected for this problem. Conservation discretization is performed on radial control volumes, and the backward Euler scheme is adopted in the time direction. It is unconditionally stable and can naturally handle variable-coefficient diffusion, with accuracy guaranteed by convergence tests.

2.3 Model Establishment

2.3.1 Governing equations and boundary conditions

The length of herbal material is 25 cm, much larger than its radius of 2 cm, so axial gradients can be neglected and only the radial direction is taken as the sole spatial variable. Here, D given in the problem is regarded as the effective water diffusion coefficient with respect to dry-basis moisture content C. Under the assumptions of homogeneous, isotropic media and concentration-gradient-driven water migration, a one-dimensional axisymmetric effective Fick diffusion model in cylindrical coordinates is adopted:

$$\frac{\partial C}{\partial t} = \frac{1}{r}\frac{\partial}{\partial r}\left(rD\frac{\partial C}{\partial r}\right) \tag{2}$$

where t is time (s), r is radial distance (m). In this problem, D depends only on C. Neglecting the enthalpy flux carried by water migration in a differential element, the energy conservation equation dominated by heat conduction is obtained:

$$\rho c_p \frac{\partial T}{\partial t} = \frac{1}{r}\frac{\partial}{\partial r}\left(rk\frac{\partial T}{\partial r}\right) \tag{3}$$

where c_p, k, T represent specific heat capacity ($J/(kg \cdot K)$), thermal conductivity ($W/(m \cdot K)$) and herbal material temperature (°C), respectively. Due to axisymmetry, the gradient at the center is zero. At the surface $r = R_0$, heat and water exchange with the drying chamber occurs by convection, i.e., third-type boundary conditions:

$$\left.\frac{\partial T}{\partial r}\right|_{r=0} = 0, \quad \left.\frac{\partial C}{\partial r}\right|_{r=0} = 0 \tag{4}$$

$$-k\left.\frac{\partial T}{\partial r}\right|_{r=R_0} = h\left(T|_{r=R_0} - T_\infty\right) \tag{5}$$

$$-D\left.\frac{\partial C}{\partial r}\right|_{r=R_0} = h_m\left(C|_{r=R_0} - C_\infty\right) \tag{6}$$

where h and h_m are surface convective heat transfer coefficient ($W/(m^2 \cdot K)$) and convective mass transfer coefficient (m/s). T_∞ and C_∞ are drying chamber air temperature (°C) and water concentration (kg/kg). At the initial moment, temperature and moisture content are uniformly distributed along the radial direction:

$$T(r,0) = T_0 = 28°C, \quad C(r,0) = C_0 = 2.55 \text{ kg/kg} \tag{7}$$

2.3.2 Thermophysical relations, characteristic time and normalized coordinates

Thermophysical properties of herbal materials are taken as constants in the preheating equilibrium stage:

$$\rho = 820 \text{ kg/m}^3, \quad c_p = 2600 \text{ J/(kg} \cdot \text{K)}, \quad k = 0.36 \text{ W/(m} \cdot \text{K)} \tag{8}$$

The water diffusion coefficient varies exponentially with moisture content:

$$D(C) = 7 \times 10^{-9} exp\left(-\frac{0.89}{C}\right) \tag{9}$$

where C is dry-basis moisture content (kg/kg). D increases monotonically with moisture content and remains positive. Its variation within the preheating stage is less than 21%, indicating weak nonlinearity, which can be linearized at the previous time level. The characteristic time scales for heat and mass transfer are:

$$\tau_T = \frac{R_0^2}{\alpha} = \frac{R_0^2 \rho c_p}{k} \approx 2.4 \times 10^3 \text{ s}, \quad \tau_C = \frac{R_0^2}{D} \approx 8.1 \times 10^4 \text{ s} \tag{10}$$

where $\alpha = k/(\rho c_p)$ is thermal diffusivity (m^2/s). Equation (10) shows that the temperature field fully develops within about 40 min, while the water concentration field requires more than 22 h. Thus within 1800 s, the temperature field is fully developed and water migration only occurs within approximately 0.3 cm of the surface layer. To uniformly handle geometric shrinkage and improve surface grid resolution, a normalized radial coordinate is introduced:

$$\xi = \frac{r}{R(t)} \in [0,1] \tag{11}$$

where ξ is normalized radial coordinate and R(t) is the current radius of herbal material (m). $R(t) \equiv R_0$ for this problem. The radial derivative under this coordinate satisfies:

$$\frac{\partial}{\partial r} = \frac{1}{R}\frac{\partial}{\partial \xi}, \quad r\frac{\partial}{\partial r} = \xi\frac{\partial}{\partial \xi} \tag{12}$$

Substitute Eq.(11) and Eq.(12) into Eq.(2) and Eq.(3) to obtain governing equations under normalized coordinates:

$$\frac{\partial C}{\partial t} = \frac{1}{\xi R^2}\frac{\partial}{\partial \xi}\left(D\xi\frac{\partial C}{\partial \xi}\right) \tag{13}$$

$$\rho c_p \frac{\partial T}{\partial t} = \frac{1}{\xi R^2}\frac{\partial}{\partial \xi}\left(k\xi\frac{\partial T}{\partial \xi}\right) \tag{14}$$

The corresponding boundary conditions are rewritten as:

$$\left.\frac{\partial C}{\partial \xi}\right|_{\xi=0} = 0, \quad -\frac{D}{R}\left.\frac{\partial C}{\partial \xi}\right|_{\xi=1} = h_m\left(C|_{\xi=1} - C_\infty\right) \tag{15}$$

From Eq.(13) to Eq.(15), R is constant when dimensional change of herbal material is neglected.

2.3.3 Finite volume discretization and fully implicit solution

Divide $\xi \in [0,1]$ uniformly into N control volumes. The center of the i-th control volume is $\xi_i = (i + 0.5)/N$, with inner and outer interfaces $\xi_{i-1/2} = i/N$ and $\xi_{i+1/2} = (i + 1)/N$. Its volume and interface area are:

$$V_i = \pi R^2\left(\xi_{i+1/2}^2 - \xi_{i-1/2}^2\right), \quad A_{i\pm1/2} = 2\pi R\xi_{i\pm1/2} \tag{16}$$

where the axial length is taken as unit length (L = 1). If actual axial length is retained, both volume and area scale by L, and this factor cancels out in conservation equations without affecting results.

Integrate Eq.(13) over the control volume. Diffusion coefficients at interfaces take the arithmetic average of adjacent control volumes to obtain the semi-discrete conservation form:

$$V_i\frac{dC_i}{dt} = \frac{A_{i-1/2}D_{i-1/2}}{R\Delta\xi}(C_{i-1} - C_i) + \frac{A_{i+1/2}D_{i+1/2}}{R\Delta\xi}(C_{i+1} - C_i) \tag{17}$$

where $\Delta\xi = 1/N$ is normalized grid step. Substitute Eq.(16) and cancel the common factor $2\pi R^2$. The temperature equation is processed similarly, and Eq.(15) is used to replace the outer interface flux of the surface control volume:

$$\frac{dC_i}{dt} = \frac{2N^2}{R^2(2i+1)}\left[iD_{i-1/2}(C_{i-1} - C_i) + (i+1)D_{i+1/2}(C_{i+1} - C_i)\right] \tag{18}$$

$$\frac{dT_i}{dt} = \frac{2N^2}{\rho c_p R^2(2i+1)}\left[ik_{i-1/2}(T_{i-1} - T_i) + (i+1)k_{i+1/2}(T_{i+1} - T_i)\right] \tag{19}$$

For $i = 0$, the inner interface coefficient automatically satisfies central symmetry. The center of the outermost control volume $i = N - 1$ is located at $\xi_{N-1} = 1 - 1/(2N)$, which is half a grid spacing δ away from the true surface R. Directly

taking its center value as the surface value will introduce O(h) truncation error. Therefore, the half-grid conduction (mass transfer) resistance from the surface to control volume center is connected in series with surface convective resistance, and equivalent coefficients h_{eff}, $h_{m,eff}$ are used instead of h, h_m. For $i = N - 1$, the outer interface coefficient takes Rh_{eff} (temperature) and $Rh_{m,eff}$ (moisture), with source terms $Rh_{eff}T_\infty$ and $Rh_{m,eff}C_\infty$. The backward Euler scheme is adopted for temporal discretization, and thermophysical properties are linearized at the previous time level, yielding the linear system at time level n + 1:

$$\frac{C_i^{n+1}-C_i^n}{\Delta t} = \frac{2N^2}{R^2(2i+1)}\left[iD_{i-1/2}^n(C_{i-1}^{n+1} - C_i^{n+1}) + (i+1)D_{i+1/2}^n(C_{i+1}^{n+1} - C_i^{n+1})\right] \tag{20}$$

Rearrange into standard tridiagonal form:

$$-a_iC_{i-1}^{n+1} + b_iC_i^{n+1} - c_iC_{i+1}^{n+1} = d_i \tag{21}$$

where coefficients are defined as:

$$a_i = \Delta tGiD_{i-1/2}^n, \quad c_i = \Delta tG(i+1)D_{i+1/2}^n, \quad b_i = (2i+1) + a_i + c_i, \quad d_i = (2i+1)C_i^n \tag{22}$$

$$G = \frac{2N^2}{R^2}, \begin{cases} a_{N-1} = \Delta tG(N-1)D_{N-3/2}^n \\ b_{N-1} = (2N-1) + a_{N-1} + \Delta tGRh_{m,\text{eff}} \\ d_{N-1} = (2N-1)C_{N-1}^n + \Delta tGRh_{m,\text{eff}}C_\infty \end{cases} \tag{22}$$

The equivalent coefficients of the outermost control volume are obtained by series connection of half-grid resistance and surface convective resistance:

$$\delta = \frac{R}{2N}, \quad h_{\text{eff}} = \frac{hk}{k+h\delta}, \quad h_{m,\text{eff}} = \frac{h_mD}{D+h_m\delta} \tag{23}$$

where δ = R/(2N) is the half-grid distance from the center of the outermost control volume to the true surface; k and D take thermophysical values at the current time level of the outermost control volume. The temperature equation has an identical tridiagonal structure, only replacing D with k, 2i + 1 with $\rho c_p(2i + 1)$, and replacing Rh_m, source term Rh_mC_∞ in boundary terms with Rh_{eff}, $Rh_{eff}T_\infty$. Eq.(21) to (23) are solved by the Thomas algorithm, with single-step computational cost of O(N). A time step of 1 s consistent with output resolution can be adopted. Core parameter settings of the numerical model are listed in Table 2.

Table 2 Model Parameter Settings

Parameter	Description	Value	Basis
N	Number of radial control volumes	128	Grid convergence test
Δt	Time step (s)	0.25	Time step convergence test

3 RESULTS

3.1 Model Solution

Based on the above model, the drying chamber temperature and humidity sequence from Attachment 1 and thermophysical parameters are used for solution. The calculation environment is Python 3.12, and numerical calculation relies on the band matrix solver in NumPy and SciPy. Core parameters are set as control volume number N = 128, time step Δt = 0.25s, and other parameters are shown in Table 2. The solved results are shown below. Table 3 and Table 4 present herbal material temperature and water concentration at specified moments and positions within 30 min.

Table 3 Herbal Material Temperature (°C) Within 30 Minutes

Time/s	0 cm	0.5 cm	1 cm	1.5 cm	2 cm
100	28.0001	28.0004	28.0041	28.0326	28.1794
300	28.0408	28.0635	28.1513	28.3678	28.8477
600	28.4531	28.5359	28.8036	29.3153	30.1641
900	29.3238	29.4578	29.8749	30.6154	31.7292
1200	30.5419	30.7091	31.2216	32.1116	33.4262
1500	31.9947	32.1859	32.7651	33.7452	35.1191
1800	33.5742	33.7710	34.3631	35.3610	36.7841

Table 4 Herbal Material Water Concentration (kg/kg) Within 30 Minutes

Time/s	0 cm	0.5 cm	1 cm	1.5 cm	2 cm
100	2.5500	2.5500	2.5500	2.5500	2.2500
300	2.5500	2.5500	2.5500	2.5492	2.0525
600	2.5500	2.5500	2.5500	2.5352	1.8782
900	2.5500	2.5500	2.5497	2.5044	1.7557
1200	2.5500	2.5500	2.5482	2.4644	1.6594
1500	2.5500	2.5499	2.5445	2.4205	1.5795
1800	2.5500	2.5497	2.5383	2.3754	1.5109

It can be seen from Table 3 that the herbal material temperature gradually decreases from the surface to the center. At 1800 s, the center and surface temperatures are 33.5742 °C and 36.7841 °C respectively, with an internal-external temperature difference of 3.21 °C, and the temperature field approaches quasi-steady state. According to Table 4, water

concentration within 1 cm basically maintains the initial value at 1800 s, and water migration is only limited to the surface layer of about 0.5 cm, consistent with the characteristic time scale estimation given in Eq.(10). Radial profiles of temperature and water concentration at typical moments are shown in Figure 1.

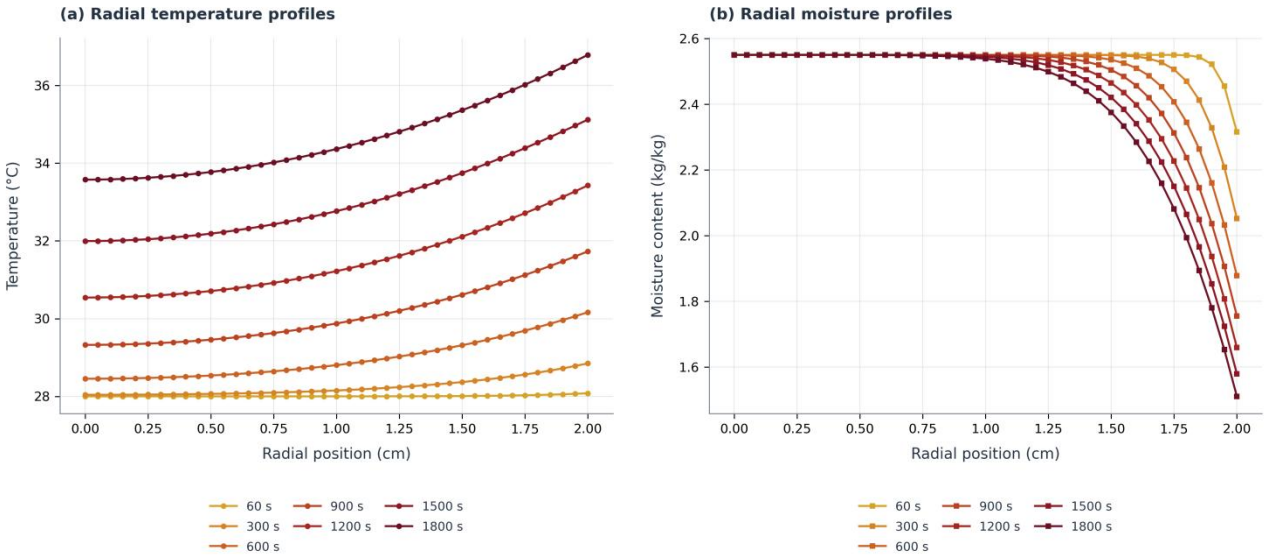


Figure 1 Radial Profiles of Temperature and Water Concentration at Typical Moments: (a) Temperature Radial Profile; (b) Water Concentration Radial Profile

It can be observed from Figure 1 that the temperature profile gradually flattens from the initial "high outside, low inside" distribution. The water concentration profile always maintains the pattern of "flat center, dropping surface", and the drop front propagates inward from the surface over time. The surface temperature is always higher than the center temperature, and the surface drying flux reaches its peak at approximately $t \approx 100s$ and then slowly decays, corresponding to the reduction of mass transfer driving force caused by the drop of surface water concentration.
Synthesizing the above results, at 1800 s, the center temperature is 33.5742 °C, the surface temperature is 36.7841 °C, the surface water concentration drops to 1.5109 kg/kg, and the center moisture content remains almost unchanged.

3.2 Model Verification

The reliability of solution results depends on the validity of the numerical scheme. In this section, convergence tests are performed for time step and spatial grid. Then numerical solutions under constant environmental conditions are compared with analytical series solutions for cylindrical unsteady heat conduction. The verification results are shown in Figure 2.

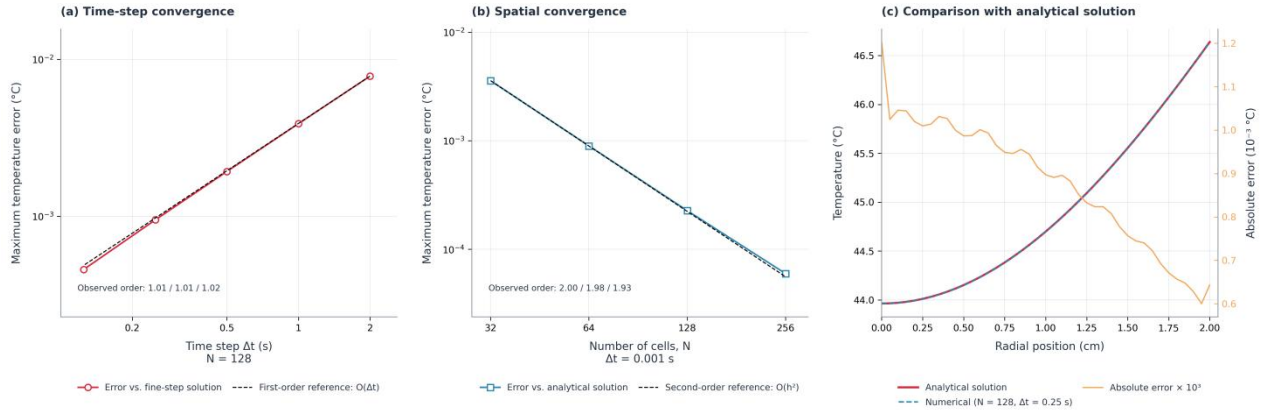


Figure 2 Convergence of Numerical Scheme and Comparison with Analytical Solution: (a) Time Step Convergence; (b) Spatial Convergence; (c) Comparison with Analytical Solution

As shown in Figure 2, with fixed N = 128, when Δt decreases from 2.0 s to 0.125 s, the maximum temperature deviation, referenced to the ultra-fine time step solution ($\Delta t = 0.0078125s$) on the same grid, decreases monotonically with first-order accuracy (measured order: 1.01 ~ 1.05). With fixed $\Delta t = 0.001s$, as the number of control volumes N increases from 32 to 256, the maximum temperature deviation referenced to analytical series solutions converges rapidly with second-order accuracy (measured order: 1.93 ~ 2.00). At 1800 s, under production parameters (N =

$128, \Delta t = 0.25\text{s}$), the absolute deviation between numerical solution and analytical series solution is controlled at the order of 10^{-3} °C (maximum 1.20×10^{-3} °C).

The above verification indicates that results including center temperature 33.5742 °C, surface temperature 36.7841 °C and surface water concentration 1.5109 kg/kg are not artifacts of discretization errors. The temperature numerical solution agrees with analytical series solutions at the magnitude of 10^{-3} °C. The water concentration field passes grid and time step convergence tests to verify its numerical stability. The two fields in the preheating equilibrium stage are reliably characterized.

4 CONCLUSIONS

This paper constructs a one-dimensional axisymmetric heat-mass coupled diffusion numerical model for the preheating-balance stage of cylindrical Chinese herbal medicine hot-air drying. By pre-processing time-varying hot-air environmental data with linear interpolation, non-physical numerical oscillations caused by step-form boundary input are eliminated. The fully-implicit finite volume method combined with the Thomas algorithm is adopted to solve transient temperature and moisture fields. Numerical results reveal that temperature rises rapidly inside the material during preheating; at 1800 s, the center temperature is 33.5742 °C and the surface temperature reaches 36.7841 °C, while moisture migration is restricted to a thin surface layer of 0.5 cm. Grid-independence tests, time-step convergence verification and comparison with analytical heat-conduction solutions prove the reliability of the established model. The present simulation framework can serve as a low-cost auxiliary tool for preheating-parameter optimization of cylindrical herbal materials, and it is technically feasible to provide reference values of internal temperature-moisture distribution for actual hot-air drying craft debugging.

Nevertheless, the current work adopts constant thermophysical parameters and fixed-radius geometry, only focusing on the independent preheating-balance phase without coupling the subsequent formal drying process. In follow-up research, temperature- and moisture-dependent variable-property relations will be introduced to extend the model to the full hot-air drying cycle. Axial terms will be supplemented to improve the geometric description accuracy, and physical drying experiments will be carried out to obtain measured field data for parameter correction. On this basis, further sensitivity analysis of preheating-control parameters will be completed to promote the practical application of this simulation method in the actual production of Chinese herbal medicine drying.

COMPETING INTERESTS

The authors have no relevant financial or non-financial interests to disclose.

REFERENCES

[1] Ju H Y, Zhao S H, Zhao H Y, et al. Influence of step-down relative humidity on drying characteristic and quality of hot air drying of Dioscoreae Rhizoma slices. Chinese Traditional and Herbal Drugs, 2021, 52(21): 6518-6527.

[2] Guo H L, Chen Y, Xu W, et al. Assessment of Drying Kinetics, Textural and Aroma Attributes of Mentha haplocalyx Leaves during the Hot Air Thin-Layer Drying Process. Foods, 2022, 11(6): 784.

[3] Yin N, Luo J, Wang C, et al. Comprehensive Evaluation of the Effects of Hot Air Drying Temperature on the Chemical Composition, Flavor Characteristics and Biological Activity of Houttuynia cordata Thunb. Foods, 2025, 14(11): 1962.

[4] van der Sman R G M, Curatolo M, Teresi L. Analytical and numerical solutions of pore formation in elastic food materials during dehydration. Current Research in Food Science, 2024, 8: 100762.

[5] Zhang C, Wang Z, Tian B, et al. Integrated analysis of internal moisture diffusion and surface moisture evaporation in the surface hardening phenomena of yam slices. Food Research International, 2025, 221: 117423.

[6] Wang X H, Wang X C, Tang P Y, et al. Current research status and application prospect of numerical simulation in traditional Chinese medicine drying. China Journal of Chinese Materia Medica, 2023, 48(13): 3440-3447.

[7] Yang K, Han H T, Liu J Y, et al. Application progress of ultrasound in the production and processing of traditional Chinese herbal medicines. Ultrasonics Sonochemistry, 2024, 111: 107158.

[8] Nwakuba N, Ezeanya N, Horsfall I T, et al. Heat and moisture transport in okra cylinders with shrinkage effects under solar drying: a multiphysics-based simulation approach. Sustainable Food Technology, 2025, 3(2): 520-536.

[9] Chen K, Torki M, Ghanbarian D, et al. Numerical simulation and study on heat and mass transfer in a hybrid ultrasound/convective dryer. Journal of Food Science and Technology, 2024, 61(6): 1094-1104.

[10] Welsh Z G, Simpson M J, Khan M I H, et al. Generalized moisture diffusivity for food drying through multiscale modeling. Journal of Food Engineering, 2023, 340: 111309.